Rectification currents in two-dimensional artificial channels

Fabio Marchesoni[1,2] and Sergey Savel'ev[2]
[1]*Dipartimento di Fisica, Università di Camerino, I-62032 Camerino, Italy*
[2]*Department of Physics, Loughborough University, Loughborough LE11 3TU, United Kingdom*
(Received 10 April 2009; published 17 July 2009)

Driven transport of noninteracting Brownian particles in two-dimensional asymmetric channels is investigated by fully accounting for longitudinal and transverse diffusions. *Bona fide* two-dimensional rectification effects are reported, which cannot be explained by an approximate Fick-Jacobs kinetics, such as the characteristic curve of the current pumped by a transverse ac bias and the selective gating exerted by a transverse ac bias on a driven longitudinal current. Possible experimental demonstrations of these effects in superconducting devices are also discussed.

DOI: 10.1103/PhysRevE.80.011120 PACS number(s): 05.40.−a, 02.50.Ey, 05.60.Cd

I. INTRODUCTION

Transport of overdamped (massless) particles in channels of finite cross section has become a hot topic in the technology of both natural [1] and artificial microporous media [2]. Due to transverse diffusion, i.e., diffusion orthogonal to the channel axis, the particle current can strongly depend on the actual channel geometry [3].

In the following we consider for simplicity a two-dimensional (2D) channel directed along the x axis and mirror symmetric with respect to it. At equilibrium with temperature T, a particle suspended inside such channel executes a constrained 2D Brownian motion with coordinates $\vec{r}=(x,y)$, the transverse coordinate y being confined between periodic boundaries $\pm w(x)$ with $w(x+x_L)=w(x)$. For narrow channels, $w(x)\ll x_L$, and small-amplitude boundary modulations, $|w'(x)|\ll 1$, one can assume that the probability density of the particle is uniformly distributed along the y axis, so that its reduced probability density $P(x,t)$ obeys the Fick-Jacobs (FJ) kinetic equation [4,5],

$$\frac{\partial}{\partial t}P(x,t)=\frac{\partial}{\partial x}D(x)\left[\frac{\partial}{\partial x}+\frac{V_L'(x)}{kT}\right]P(x,t). \tag{1}$$

The problem of the correct x dependence of the diffusion coefficient $D(x)$ is still matter of debate [5–7], but it has no bearing on this work. Under the additional restrictions $|w'(x)|\ll kT/Fx_L$ and $|w'(x)|\ll kT/Gy_L$ [8], the effective potential $V_L(x)$ can be written as the superposition,

$$V_L(x)=-Fx-kT\ln\left[2\frac{kT}{G}\sinh\frac{Gw(x)}{kT}\right], \tag{2}$$

of a drift term corresponding to the longitudinal force F [9] and a logarithmic term, linear in T, which depends on the boundary and the transverse force G applied perpendicularly to it [10]. For $G\to 0$ this second term boils down to the more conventional "entropic" term $-kT\ln w(x)$ [4,5].

The design and operation conditions of today's artificial channels are often incompatible with the assumptions of the FJ kinetics [2]: (i) sharply tailored profiles with large $|w'(x)|$ are commonly adopted in current nanotechnology experiments; (ii) effective rectification in asymmetric channels, $w(x-x_0)\neq w(-x-x_0)$ for all $x_0\in[0,x_L]$, requires sharply modulated boundaries; and (iii) in the presence of external dc or ac drives, as is often the case, transverse relaxation can hardly be instantaneous. The analysis of Brownian transport in a 2D channel must thus be pursued beyond the reduced FJ theory.

This paper is organized as follows. In Sec. II we introduce a simple model for a 2D asymmetric period channel with reflecting walls. In Sec. III a dc drive, F, is applied to a Brownian particle suspended in the channel; the particle mobility in the opposite direction is computed as a function of the drive amplitude and for different geometries of the channel unit cell. A comparison of the two mobility curves allows us to predict intensity and orientation of the rocked ratchet current induced by a low-frequency longitudinal ac drive. In Sec. IV an ac drive, G, is applied perpendicularly to the channel axis. The Brownian particle perceives an effective one-dimensional (1D) pulsated ratchet, so that it gets rectified in the direction opposite to the configuration of Sec. III. The combination of longitudinal and transverse diffusions determines the intensity of the directed current in the channel. In Sec. V the mobility of a longitudinally driven Brownian particle in a perpendicularly pulsated channel is investigated for different drive intensities and pulsation frequencies. The ensuing gating current develops outstanding commensuration peaks, which are the signature of the interplay of longitudinal and transverse forces. Possible applications to the design and operation of superconducting devices are briefly discussed in Sec. VI.

II. MODEL

The 2D dynamics of an overdamped Brownian particle is represented by the Langevin equation

$$d\vec{r}/dt=-F\vec{e}_x-G\vec{e}_y+\sqrt{kT}\vec{\xi}(t), \tag{3}$$

where $\vec{e}_x,\vec{e}_y$ are the unit vectors along the x,y axes and $\vec{\xi}(t)=[\xi_x(t),\xi_y(t)]$ are zero-mean white Gaussian noises with autocorrelation functions

$$\langle\xi_i(t)\xi_j(t')\rangle=2\delta_{ij}\delta(t-t')$$

for $i,j=x,y$. The Langevin equation [Eq. (3)] has been numerically integrated for different arrangements of the external forces. Typically the longitudinal force was chosen con-

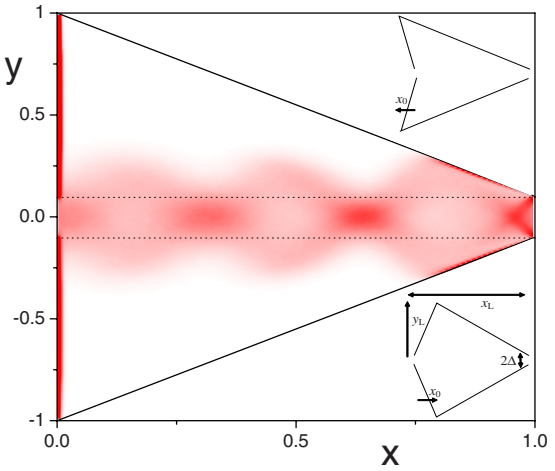

FIG. 1. (Color online) Brownian particle in a 2D periodic channel directed along the x axis and with periodically modulated boundary $w(x)=(y_L-\Delta)(x/x_0)+\Delta$ for $0<x<x_0$ and $=y_L-(y_L-\Delta)(x-x_0)/(x_L-x_0)$ for $x_0<x<x_L$. In our simulations the cell geometry was varied by changing x_0 for fixed $x_L=y_L=1$ and $\Delta=0.1$: $x_0=0$ (main panel), 0.2 (bottom, right), and -0.1 (top, right). The stationary distributions of a driven particle in one-cell reduced representation (also called particle beam) are shown for $F=2$, $G=5$, $T=0.005$, and $\nu_\Omega=\nu_6=6$ (see text).

stant and the transverse force was sinusoidally modulated in time, $G(t)=G\cos(\Omega t)$. The results reported here are restricted to the case of reflecting boundaries [11], described by the piecewise linear function $w(x)$, with period x_L and maximum width y_L, sketched in Fig. 1. The width of the bottlenecks was kept narrow, $\Delta \ll y_L$. The degree of $x \to -x$ asymmetry of the channel profile is controlled by the tunable parameter $x_0/x_L \in [0,0.5]$ (rhombic symmetric cells for $x_0/x_L=0.5$ and triangular cells for $x_0=0$ [12]). By introducing dimensionless units, $x \to x/x_L$, $y \to y/y_L$, and $t \to (kT/x_L y_L)t$, one proves that, for any given geometry, the transport dynamics [Eq. (3)] is controlled solely by the rescaled forces Fx_L/kT and Gy_L/kT and possibly by $x_L y_L \Omega/kT$. In our simulation the cell aspect ratio y_L/x_L was set to 1, with $x_L=y_L=1$, so that neither FJ conditions apply.

III. ROCKED CHANNELS

We start our analysis with the simplest case of a purely longitudinal steady flow driven by a dc force F in the absence of transverse bias, $G=0$. In Fig. 2 we plot the corresponding mobility functions $\mu_\pm(|F|)$ defined as $\mu_+(|F|)=\mu(F)$ for $F \geq 0$ and $\mu_-(|F|)=\mu(-F)$ for $F \leq 0$, with $\mu(F)=v/F$ and $v \equiv \langle \dot{x} \rangle$. In shorthand notation the $|\cdots|$ sign in $\mu_\pm$ is dropped. Due to our channel geometry, $\mu_\pm$ represent the mobilities in the easy and hard directions, respectively, that is, $\mu_+(F)>\mu_-(F)$ with $\mu_+(0)=\mu_-(0)$. Note that $\mu_\pm(0)$ is almost independent of x_0. As a consequence, a low-frequency time periodic, say, sinusoidal force $F(t)$, would rectify the particle motion in the easy direction (rocked ratchet [13]). Note that for asymmetric channels, $x_0 \neq 0.5$, $\mu'_+(0)=-\mu'_-(0)>0$ [11], hence the minimum of μ_- for $0<x_0<0.5$.

All curve pairs $\mu_\pm(F)$ approach the expected asymptotic value $\mu_\pm(\infty)=1$, with the exception of μ_- at $x_0=0$. To clarify

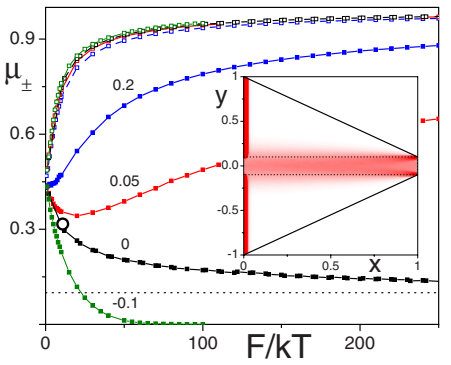

FIG. 2. (Color online) Mobilities μ_+ (open symbols) and μ_- (solid symbols) versus F/kT in the periodic 2D channel of Fig. 1 for $G=0$, $T=0.1$, and different values of the asymmetry parameter x_0 (rocked channel). The $\mu_\pm$ curves for $x_0=-0.1$ are shown for a comparison. The dotted line represents the asymptote $\mu_-(\infty)=0.1$ (see text). Inset: particle beam corresponding to the open circle on the μ_- curve for $x_0=0$.

this point we displayed here a pair of mobility curves for $x_0<0$ too: as F pushes in the hard direction, the particle gets trapped inside the $|x_0|$ deep pockets above and below the bottleneck (Fig. 1, top right inset), so that $\mu_-(F)$ gets suppressed by the Arrhenius factor $\exp(-Fx_0/kT)$ [14]. The μ_- curve for $x_0=0$ thus acts as a separatrix between the μ_- curves pointing upward toward one, for $x_0>0$, and those decaying to zero for $x_0<0$.

The F dependence of $\mu_-(F)$ at $x_0=0$ is remarkable. We found that it approaches the horizontal asymptote

$$\mu_-(\infty) = \Delta/y_L$$

with power law decay

$$\mu_-(F) - \mu_-(\infty) \propto (kT/|F|)^{1/2}.$$

This behavior cannot be surely explained in terms of the FJ kinetics [8]. A simple phenomenological argument convinced us that our numerical findings were consistent. Subject to the longitudinal force pointing in the negative direction, the particle gets pressed against the bottom of the triangular cell (see the inset of Fig. 2), where it keeps diffusing unhindered in the transverse direction. After it eventually squeezed its way around the edges of the opening, the particle hits the bottom of the neighboring cell to its left in a time of the order of $x_l/|F|$. During its ballistic flight, however, the particle undergoes transverse diffusion and, upon hitting the bottom of the cell, it will be scattered over a region of total radius $\Delta+\Delta_T(F)$, with

$$\Delta_T(F) \simeq \sqrt{2x_L kT/|F|}.$$

This is the effective radius of the bottleneck in the hard direction corrected for thermal diffusion. In agreement with our observations, $\mu_-(F)=\Delta/y_L+\Delta_T(F)/y_L$ is then the fraction of the particle actually being transported in the stationary regime.

As mentioned above the curves $\mu(F)$ versus F/kT are determined by the channel geometry alone. Moreover, $\mu_\pm(0)$ is weakly dependent on x_0 at odds with predictions based on

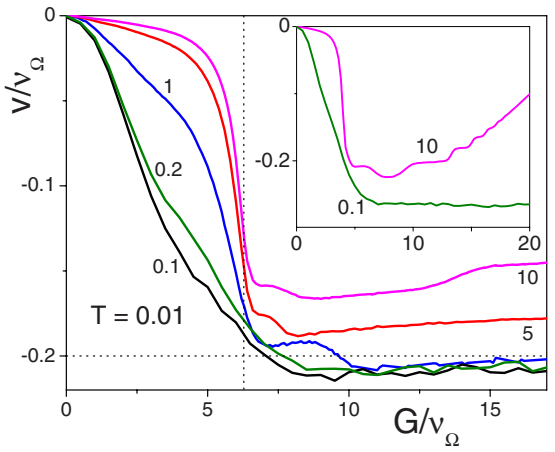

FIG. 3. (Color online) Net current v/ν_Ω vs G/ν_Ω in the channel of Fig. 1 with $x_0=0$ for $F=0$, $T=0.01$, and pulsated at different ν_Ω (legends). The dotted lines represent the horizontal asymptote $v(\infty)/\nu_\Omega=-0.2$ for $\nu_\Omega \lesssim 1$ and the threshold $G_{\rm th}/\nu_\Omega=2\pi$ (see text). Inset: same as in the main panel but for a square wave form of the pulsation $G(t)$.

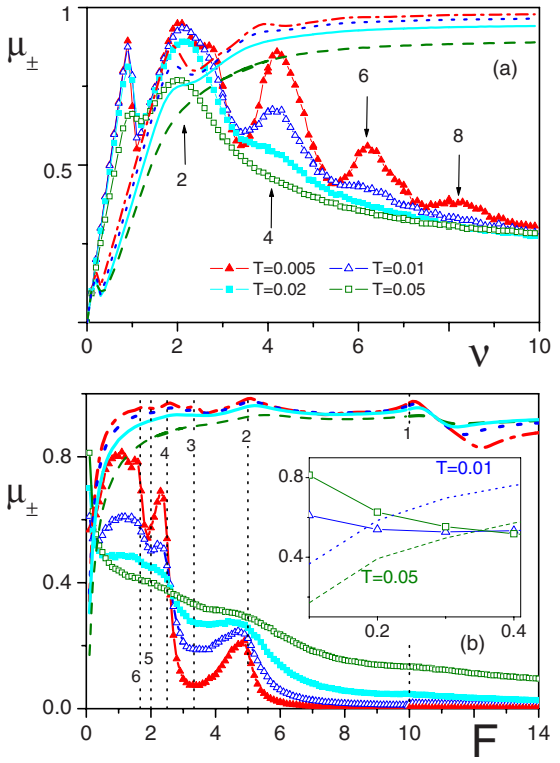

FIG. 4. (Color online) Mobilities μ_+ (dots) and μ_+ (squares) in the channel of Fig. 1 with $x_0=0$ for different T; the channel is subjected to a sinusoidal transverse force $G(t)$ and a longitudinal dc drive F (gating configuration). (a) $\mu_\pm$ versus ν_Ω for $G=5$ and $F=2$; (b) $\mu_\pm$ versus F for $G=5$ and $\nu_\Omega=5$. The predicted peak positions, ν_n and F_n, are marked by vertical arrows and dotted lines, respectively, with the relevant index n. T values are 0.005 (solid triangles and dashed-dotted curves), 0.01 (empty triangles and dotted curves), 0.02 (solid squares and solid curves), and 0.05 (empty squares and dashed curves). (Inset: low F details for two values of T.)

the FJ equation [Eq. (1)] [13]. We confirmed this observation by looking at the mean first passage time τ for an unbiased particle placed in the midsection of a bottleneck to diffuse across an adjacent bottleneck to its right or left alike. Our numerical estimates for τ satisfied the identity $\mu_\pm(0)=x_L^2/kT\tau$, proved indeed proportional to kT, as expected, and almost insensitive to x_0.

IV. PULSATED CHANNELS

We consider now the case of a channel transversally biased by a sinusoidal force $G(t)$ with frequency $\nu_\Omega=\Omega/2\pi$ in the absence of longitudinal drives, $F=0$. In terms of the FJ kinetic equation the particle would move in a ratchet potential $V_L(x)$ [Eq. (2)], subject to time pulsation with frequency $2\nu_\Omega$ (pulsated ratchet): rectification would thus occur in the hard direction and vanish for $G\to\infty$ [15].

Our numerical simulation delivers a rather different picture. In Fig. 3 we only report data for the most asymmetric channel geometry, $x_0=0$. The curves of the net current v versus G are indeed negative for all pulsation frequencies but, when plotted in units of ν_Ω, their amplitudes exhibit a sharp step at approximately the same G/ν_Ω and, for low ν_Ω, approach the same horizontal asymptote $v(\infty)/\nu_\Omega$.

This behavior is a manifestation of the interplay of transverse and longitudinal diffusions. The particle stands a better chance to diffuse sidewise through the bottleneck to its left during a half bias cycle if G is intense enough to squeeze it toward the corners of the triangular channel cell. This happens when the amplitude of the free particle transverse oscillations equals the maximum width of the cell, namely, for $G_{\rm th}/\Omega=y_L$. For larger G, the particle is swept up and down close to the flat bottom of the cell. If the particle is allowed to diffuse distances *longer* than Δ during one half bias period, then the argument introduced above to estimate $\mu_-(\infty)$ applies again: the particle leaves the cell at each passage with probability Δ/y_L. In conclusion, we predict

$$v(\infty)/\nu_\Omega = -2\Delta x_L/y_L$$

for $\nu_\Omega \lesssim kT/\Delta^2$. Both estimates for $G_{\rm th}$ and $v(\infty)$ agree quite closely with the simulation data of Fig. 3 for low ν_Ω. On increasing ν_Ω the steps at $G_{\rm th}$ get sharper, but for $\nu_\Omega > 1$ the tail of v/ν_Ω approaches zero.

The bump appearing next to the onset step is a finite size effect that depends on the details of the cell geometry. Finite size effects are even stronger in the case of a square waveform, $G(t)$, with equal amplitude, G, and frequency, ν_Ω, as proven by the steplike decay of $v(G)$ in the inset of Fig. 3 for large ν_Ω.

V. GATING IN PULSATED CHANNELS

We finally analyze the action of a periodic bias $G(t)$ on the dc driven along the asymmetric channel with $x_0=0$. In Fig. 4 we plot the mobilities $\mu_\pm$ versus ν_Ω at constants G and F [panel (a)] and versus F at constants G and ν_Ω [panel (b)]. In FJ kinetic scheme [Eqs. (1) and (2)] the particle flow across the channel bottlenecks would be subjected to the optimal gating condition [16] when the particle crosses a unit

cell with ballistic time equal (or close) to an integer number of half G periods. Consequently, on ignoring small noise effects, $\mu_{\pm}$ peaks ought to occur for $\nu_\Omega = \nu_n$ in Fig. 4(a) and $F = F_n$ in Fig. 4(b), with

$$\nu_n = nF/2x_L, \quad F_n = 2x_L\nu_\Omega/n, \quad n = 1,2, \ldots . \tag{4}$$

In our simulations, however, peaks corresponding to odd n in both panels are strongly suppressed.

Gating is more effective in the hard direction, where, on hitting the bottom of the cell, the particle gets sensibly delayed and therefore out of phase with $G(t)$. In the easy direction the triangular boundaries of the cell act as a funnel, thus refocusing the particle beam (i.e., the particle trajectory in the one-cell reduced representation of Fig. 1). As a consequence the peak structures are less apparent for μ_+ than μ_-.

The peak structures grow more conspicuous either on lowering the temperature or increasing the bias amplitude (not shown), being G/kT the effective control parameter. To this regard, we notice that the particle traveling along the channel tends to execute sinusoidal trajectories with amplitude G/Ω; only those hitting the bottlenecks get hindered. Therefore, the gating effect is expected to set on for $G/\Omega \gtrsim \Delta$. [Note that in Fig. 4(b) $G \gtrsim 3$ and in Fig. 4(a) the μ_- peaks vanish for $\nu_\Omega \gtrsim 8$.] Moreover, as mentioned above, during the ballistic traversal time $x_L/|F|$ the particle beam widens with transverse diffusion radius Δ_T. The beam radius must be sensibly smaller than the bottleneck radius for gating to become appreciable, $\Delta_T < \Delta$. This happens for

$$kT \lesssim kT_c = (|F|/2x_L)\Delta^2.$$

[For the simulation parameters of Fig. 4(a) $kT_c = 0.01$.]

The $\mu_{\pm}$ curves in Fig. 4(b) cross one another for a certain value of the longitudinal dc force, which can be interpreted as a measure of the stopping force of the rectified current pumped by $G(t)$ at $F=0$ (Fig. 3). Above the crossing point μ_- turns upward and grows much larger than $\mu_-(0)$ at zero bias, $G=0$ (Fig. 2). Indeed, for ballistic traversal times much longer than the bias period (i.e., for low dc drives), the particle exits through the cell bottleneck regardless of the gating conditions [Eq. (4)]. A mobility enhancement is then expected for transverse modulations of the particle trajectory larger the diffusive beam radius, namely, for $F \gtrsim F_c$ with $F_c = 2x_L kT(\Omega/G)^2$, in close agreement with our simulation data.

The suppression of the odd n peaks in panels (a) and (b) of Fig. 4 is another typical property of the irreducible 2D dynamics [Eq. (3)]. When an unbiased particle beam enters a triangular cell from the right, it splits in two parallel beams as shown in the inset of Fig. 2. The bias $G(t)$ deviates the beams originating from the edges of the right bottleneck to opposite transverse directions, so that they overlap in the central lane of the channel upon entering the cell and, again, after every full $G(t)$ cycle. This means that they overlap also at the center of the bottleneck on the left only for n even (see Fig. 1), thus producing large μ_- peaks, whereas for n odd they hit the bottom of the cell and get blocked. As noticed above, such a blocking action is less effective when the beam travels from left to right; therefore, small μ_+ peaks are visible also for n even. Note that shrinking the opening, $\Delta \to 0$, while restoring ideal gating condition (4), would dramatically suppress μ_-.

The leftmost $\mu_{\pm}$ peaks in Fig. 4(a) seem to challenge this rule, as they are centered in the vicinity of ν_1. In fact, this is a finite size effect, which depends on the cell geometry. For large G/ν_Ω the beams run parallel to the boundaries and then refocus at the center of the cell bottom after a time not much longer than one half bias period, i.e., for $\nu_\Omega \lesssim \nu_1$. This and more details will be discussed somewhere else.

VI. CONCLUSIONS

In this paper we have shown how the interplay of transverse and longitudinal diffusions affects the particle current flowing in an asymmetric periodic channel driven by external forces either constant or periodic in time. We detected boundary effects that cannot be reproduced in the context of a reduced 1D kinetics at times not even qualitatively. Such effects suggest design geometries and operation conditions for artificial 2D channels, with applications to colloidal systems, cold atoms in optical lattices, and magnetic vortices in superconducting devices to mention a few [2].

Superconducting ratchet devices [17] are attracting growing interest because of their potential applications to the operation of flux qubits as well as the suppression of magnetic noise in active [e.g., superconducting quantum interferometric device (SQUIDs)] and passive (e.g., rf filters) superconducting devices. Vortex channels are ideal candidates to experimentally demonstrate the entropic transport effects discussed in this paper. Indeed, artificial vortex ratchets can be fabricated by etching asymmetric tracks of any shape on a superconducting surface [18,19]. Magnetic vortices are trapped in such channels with binding energies of the order of $\Phi_0^2 L_t/\lambda^2$, where Φ_0 is the magnetic flux quantum, λ is the London penetration depth, and L_t is the depth of the channel. The channel boundaries are as thin as one superconducting coherence length $\xi \sim 10$ Å, which is by far the shortest length scale in the system. Moreover, vortex densities can be readily controlled by tuning an external out-of-plane magnetic field H. In the dilute limit, $H \lesssim \Phi_0/\lambda^2$, the vortex-vortex interactions become negligible, so that the properties of single particle transport in 2D are not overshadowed by many-body effects. dc and ac drives can be easily implemented as Lorentz forces generated by independently injected currents either perpendicular or parallel to the vortex channel, corresponding to the F and G drives, respectively, introduced in our 2D channel geometries. Entropic rectification can considerably improve both controllability and efficiency of vortex ratchets.

ACKNOWLEDGMENTS

We acknowledge partial support from the ESF AQDJJ program and the EPSRC via Grants No. EP/D072581/1 and No. EP/F005482/1.

[1] B. Hille, *Ion Channels of Excitable Membranes* (Sinauer, Sunderland, 2001); J. Kärger and D. M. Ruthven, *Diffusion in Zeolites and Other Microporous Solids* (Wiley, New York, 1992).
[2] See, for a review, P. Hänggi and F. Marchesoni, Rev. Mod. Phys. **81**, 387 (2009); P. Hänggi, F. Marchesoni, and F. Nori, Ann. Phys. **14**, 51 (2005).
[3] P. S. Burada, P. Hänggi, F. Marchesoni, G. Schmid, and P. Talkner, ChemPhysChem **10**, 45 (2009).
[4] M. H. Jacobs, *Diffusion Processes* (Springer, New York, 1967).
[5] R. Zwanzig, J. Phys. Chem. **96**, 3926 (1992).
[6] D. Reguera and J. M. Rubí, Phys. Rev. E **64**, 061106 (2001).
[7] P. Kalinay and J. K. Percus, Phys. Rev. E **74**, 041203 (2006).
[8] N. Laachi, M. Kenward, E. Yariv, and K. D. Dorfman, EPL **80**, 50009 (2007).
[9] D. Reguera, G. Schmid, P. S. Burada, J. M. Rubí, P. Reimann, and P. Hänggi, Phys. Rev. Lett. **96**, 130603 (2006); P. S. Burada, G. Schmid, D. Reguera, J. M. Rubi, and P. Hänggi, Phys. Rev. E **75**, 051111 (2007).
[10] P. S. Burada, G. Schmid, D. Reguera, M. H. Vainstein, J. M. Rubí, and P. Hänggi, Phys. Rev. Lett. **101**, 130602 (2008).
[11] H. Risken, *The Fokker-Planck Equation* (Springer, Berlin, 1989).
[12] J. F. Wambaugh, C. Reichhardt, C. J. Olson, F. Marchesoni, and F. Nori, Phys. Rev. Lett. **83**, 5106 (1999).
[13] B.-Q. Ai and L.-G. Liu, Phys. Rev. E **74**, 051114 (2006).
[14] R. Eichhorn, P. Reimann, and P. Hänggi, Phys. Rev. Lett. **88**, 190601 (2002).
[15] P. Reimann, Phys. Rep. **361**, 57 (2002).
[16] S. Savel'ev, F. Marchesoni, P. Hänggi, and F. Nori, Europhys. Lett. **67**, 179 (2004); Phys. Rev. E **70**, 066109 (2004); M. Borromeo and F. Marchesoni, Chaos **15**, 026110 (2005).
[17] J. E. Villegas, S. Savel'ev, F. Nori, E. M. Gonzalez, J. V. Anguita, R. García, and J. L. Vicent, Science **302**, 1188 (2003); C. C. de Souza Silva, J. Van de Vondel, M. Morelle, and V. V. Moshchalkov, Nature (London) **440**, 651 (2006); S. Savel'ev and F. Nori, Nature Mater. **1**, 179 (2002); D. Cole, S. Bending, S. Savel'ev, A. Grigorenko, T. Tamegai, and F. Nori, *ibid.* **5**, 305 (2006); S. Ooi, S. Savel'ev, M. B. Gaifullin, T. Mochiku, K. Hirata, and F. Nori, Phys. Rev. Lett. **99**, 207003 (2007).
[18] Y. Togawa, K. Harada, T. Akashi, H. Kasai, T. Matsuda, F. Nori, A. Maeda, and A. Tonomura, Phys. Rev. Lett. **95**, 087002 (2005).
[19] K. Yu, T. W. Heitmann, C. Song, M. P. DeFeo, B. L. T. Plourde, M. B. S. Hesselberth, and P. H. Kes, Phys. Rev. B **76**, 220507(R) (2007).